Hindawi
International Journal of Energy Research
Volume 2023, Article ID 5529837, 12 pages
https://doi.org/10.1155/2023/5529837

Research Article

Surface Functionalization of Activated Carbon Cloth for Wastewater Perchlorate Adsorption-Integrated Molecular Modeling and Experimental Energy Analysis

Wei-Fan Kuan,[1,2,3,4] **Muhammad Sheraz Ahmad**,[5] **Chia-Hsun Hsieh**,[2] **Prakash Bhuyar**,[6] **Tsing-Hai Wang**,[7] **Shu-Ching Ou**,[8] **and Ching-Lung Chen**[3,5,9]

[1]*Department of Chemical and Materials Engineering, Chang Gung University, Taoyuan 33302, Taiwan*
[2]*Division of Hematology-Oncology, Department of Internal Medicine, New Taipei Municipal Tucheng Hospital (Built and Operated by Chang Gung Medical Foundation), New Taipei City 23600, Taiwan*
[3]*Center for Sustainability and Energy Technologies, Chang Gung University, Taoyuan 33302, Taiwan*
[4]*College of Environment and Resources, Ming Chi University of Technology, New Taipei City 24301, Taiwan*
[5]*Center for Environmental Sustainability and Human Health, Ming Chi University of Technology, New Taipei City 24301, Taiwan*
[6]*School of Renewable Energy, Maejo University, Chiang Mai 50290, Thailand*
[7]*Department of Chemical Engineering and Materials Science, Yuan Ze University, Chongli 320, Taiwan*
[8]*Department of Chemistry & Biochemistry, University of Delaware, Newark, DE 19713, USA*
[9]*Department of Safety, Health and Environmental Engineering, Ming Chi University of Technology, New Taipei City 24301, Taiwan*

Correspondence should be addressed to Shu-Ching Ou; ousc@udel.edu and Ching-Lung Chen; tommy@mail.mcut.edu.tw

Received 28 August 2023; Revised 4 November 2023; Accepted 13 November 2023; Published 8 December 2023

Academic Editor: Mohamed Zbair

Perchlorate (ClO_4^-) in drinking water is one of the most serious issues relating to drinking water contamination. This work reports both the experimental and computational investigation of wastewater perchlorate adsorption on surfactant-modified activated carbon cloth (ACC) in order to design an efficient water treatment system. Three different types of cationic surfactants including tetramethylammonium (TMA), benzyltrimethylammonium (BTMA), and dodecyltrimethylammonium (DDTMA) were employed in this study, and the ClO_4^- adsorption capacity of various adsorbents was determined in batch experiments for 24 hours. Among all, DDTMA-ACC exhibits the highest ClO_4^- adsorption capacity (4.5 times that of pristine ACC), the highest monolayer coverage capacity (Γ_{max}) value (0.59 mmol/g), an equilibrium adsorption constant (K_L) value (35.90 L/mmol), and the lowest ΔG_{ads} value (-26.0 KJ/mol), revealing that ClO_4^- has a stronger affinity for ACC functionalized by DDTMA than ACC functionalized by other surfactants. Molecular dynamics (MD) simulations were also conducted to illustrate the interactions among ClO_4^-, surfactants, and a model graphite surface underwater environment. The relative number density profiles and cumulative number studies demonstrate that TMA/BTMA tends to form single-layered packing near the graphite surface, while DDTMA prefers to pack in a multilayered fashion. The dense packing behavior of DDTMA on the graphite surface can enhance the ClO_4^- adsorption, showing good agreement with experimental results.

1. Introduction

Due to population growth and pollution, the global demand for clean and drinkable water has steadily increased. Globally, water contamination by anionic pollutants (NO_3^-, NO_2^-, CN^-, S^{2-}, and Cl^-) [1, 2] and heavy metals (Ni, Zn, Pb, Cr, Cu, Hg, As, and Cd) [3] is increasing, and it is essential to investigate the appropriate strategies for improving water quality and reducing water scarcity. The presence of perchlorate (ClO_4^-) in drinking water is one of the most critical issues about the contamination of source water [4]. Ingestion of perchlorate-containing water or food products would limit thyroidal iodine uptake because the size and shape of perchlorate are comparable to those of iodide (I^-)

[5]. The low level of iodine intake thus decreases the production of thyroid hormone and causes a detrimental impact on the metabolism and growth of newborns, hypothyroidism, and neurological malfunction associated with other thyroid disorders [6, 7].

Physicochemical methods like adsorption, membrane filtration, and ion exchange have been extensively investigated to remove perchlorate from contaminated water [4]. Among different strategies, adsorption is the most widely used technology due to its combined advantages of low cost, high treatment efficiency, and easy operation. Additionally, activated carbon (AC) is widely used as an adsorbent due to its high surface area and tunable surface morphology. Therefore, significant efforts have been devoted to the surface engineering of AC in order to improve the adsorption capacity [8].

For example, Chen et al. [9] functionalized a bituminous granular AC with ammonia gas and obtained 4 times higher ClO_4^- adsorption compared to a virgin counterpart. They found that the increase in ClO_4^- adsorption capacity was closely correlated to the positive surface charge, which was enhanced by increasing nitrogen content during the ammonia functionalization. The study by Cui and Atkinson [10] fabricated the AC from glycerol and acid-mediated dehydration, polymerization, and carbonization. Sulfuric acid and phosphoric acid were applied during the AC preparation. Their results demonstrated that sulfuric acid-tailored AC exhibited an extremely high surface area of 2470 $m^2\ g^{-1}$. However, the highest adsorption capacity was obtained in phosphoric acid-tailored AC, which was attributed to the higher amount of oxygen surface functional groups and the formation of surface complexation. Mahmudov et al. utilized quaternary ammonium salts as cationic surfactants to functionalize the AC and reported that its capability for ClO_4^- adsorption was significantly improved [11, 12]. The removal of ClO_4^- was found to be directly related to the surfactant chain length, which induced the formation of more positive surface charges as evidenced by zeta potential measurements.

Although surface modification on AC presents an effective approach to promoting its ClO_4^- adsorption capacity, most studies in the literature that discussed the interactions between substrate and surfactant as well as surfactant and ClO_4^- have been based on experimental observations such as kinetics and isotherm experiments that are inadequate for providing a fundamental understanding. To further support and guide experimental work, it is of interest to employ molecular simulations to examine the interaction among AC substrate, surfactants, and ClO_4^-. One of the most powerful techniques for modeling interaction behaviors between chemicals and substrates is molecular dynamics (MD) simulation [13–18]. The MD simulation method is able to analyze the movement of molecules in a complex system at the atomic level by numerically solving Newton's equation of motion [19]. Previous efforts have demonstrated that MD simulation can illustrate the adsorption state of nonionic and cationic surfactants on the low-rank coal surface [15, 20]. MD simulations can be used efficiently for the identification of adsorption sites, measurement of binding energies, elucidation of adsorption data, and optimization of adsorption processes [21]. In a recent study by Ouachtak et al. [22], MD simulation was used to investigate the adsorption behavior of methylene blue (MB) and crystal violet (CV) on green adsorbent montmorillonite @ activated carbon (Mt@AC). The RDF analysis and interaction energy calculations reveal that CV has a stronger affinity for the AC sheet and the montmorillonite framework than MB. Moreover, simulation results were found to be in good agreement with experimental adsorption isotherm measurements. MS simulations were used to evaluate the separation performance of porous C_2N and g-C_3N_4 nanosheets for the separation of NO_3^- and NO_2^- pollutants from aqueous solutions. It was reported that the hydrophilic nature of these membranes (as confirmed by RDF between O_2, H_2, and N_2 molecules) resulted in a threefold increase in self-diffusivity [23].

Attempts are being made to discover low-cost materials that can be used as green adsorbents from environmentally friendly resources without compromising efficiency. Low-cost green adsorbents can be made from a wide range of materials, such as clay, biomass waste, sawdust, and date palm charcoal [24]. Recently, orange peel waste has been utilized as a green biomass adsorbent for textile wastewater treatment and the production of biogas and biochar following regeneration and recycling. This adsorption system achieved a chemical oxygen demand (COD) of 38.56 ± 1.73%, total dissolved solids (TDS) of 29.31 ± 1.25%, and turbidity and color removal efficiencies of 91.92 ± 4.75% and 74.81 ± 3.96%, respectively [25]. Using NaOH chemically modified palm fiber (NaOH-CMDPF) waste biomass, Kumar et al. [26] achieved a high phenol removal efficiency from aquatic environments. It was reported that chemical modification with NaOH enhances phenol removal by 86% compared to raw date palm fiber (RDPF) with a removal efficiency of 81%. In another study, mesoporous-activated carbon (CSAC) prepared and activated by chitosan flakes (CS) and NaOH, respectively, was used for the adsorption of methylene blue (MB). A CSAC maximum adsorption capacity of 143.53 mg/L at 50°C was obtained by fitting to the Langmuir model [27]. A low-cost mesoporous zeolite-activated carbon (Z–AC) composite was used by Khanday et al. [28] as an effective adsorbent for dye removal. A maximum adsorption capacity of 285.71 mg/g of methylene blue was obtained at 50°C. Mesoporous activated carbon prepared from rattan (*Lacosperma secundiflorum*) hydrochar followed by NaOH activation and karanj (*Pongamia pinnata*) fruit hulls was used for adsorption of methylene blue (MB) with MB removal efficiency of 96% [29] and maximum adsorption capacities of 239.4 mg/g_{MB} with hydrochar and karanj fruit hulls, respectively [30]. Khanday et al. [31–33] utilize zeolite-hydroxyapatite oil palm ash (Z-HAP-AA), phosphoric acid-activated chitin (chitin-AC), and activated oil palm ash zeolite/chitosan composite (Z-AC/C) cross-linked beads for the adsorption of the antibiotic tetracycline, antibiotic cephalexin, and methylene blue (MB)/acid blue 29 (AB29), respectively. A maximum monolayer adsorption capacity of 186.09 mg/g_{MB}, 245.19 mg/g_{MB}, and 199.20 mg/g_{MB} was obtained at 50°C for Z-HAP-AA, chitin-AC, and Z-AC/C, respectively. Marrakchi et al. [34] used cross-linked chitosan/sepiolite composite (CS50SP50) for methylene blue and reactive orange 16 (RO 16) adsorption. At an optimum adsorbent

dosage of 0.2 g/100 mL, over a pH range of 3-11 and an initial dye concentration of 25-400 mg/l, a maximum monolayer adsorption capacity of 40.986 mg/g and 190.965 mg/g was calculated for CS50SP50 and RO 16, respectively. A pseudo-second-order kinetic was reported to have better adsorption than a pseudo-first-order kinetic.

The present study is aimed at exploring the adsorption behavior of cationic surfactants with distinct moieties on the surface of AC substrate and further investigating the correlation between surface functionalization and adsorption of anionic pollutants, i.e., ClO_4^-, from water. Most significantly, a joint experiment and MD simulation effort was carried out to study the interaction mechanisms among three species, which are rarely discussed in the literature. Different quaternary ammonium salts including tetramethylammonium (TMA), benzyltrimethylammonium (BTMA), and dodecyltrimethylammonium (DDTMA) were chosen as cationic surfactants in this study (Figure 1). Alkyl chains are bonded to the N center in TMA, which has a symmetric structure. In BTMA, a CH_2 group connects the benzyl ring to the ammonium quaternary group, while in DDTMA's ammonium quaternary group, it is attached to a 12-alkyl chain [35]. The examination of these three cationic surfactants through our integrated simulation-experimental approach will reveal the impacts of long alkyl chains and the presence of benzyl rings on adsorption behaviors onto the ACC surface, which provide a transformative impact on material design and enable the development of systems that greatly surpass the performance of conventional adsorbents for perchlorate removal in wastewater.

2. Experimental

2.1. Materials. All cationic surfactants used in this study were procured from Alfa Aesar Company (United States) and utilized without further purification. The aqueous solution was prepared using deionized water with a resistivity greater than 18 ΩM cm and distilled water. The standard perchlorate (ClO_4^-) solution was acquired from SPEX CertiPrep (USA). Stock solutions of sodium perchlorate (>98%, Sigma-Aldrich, USA) and sodium hydroxide (>97%, Fisher Scientific, USA) were prepared by individually dissolving metal salts into deionized water. In ion chromatography analysis, a 50% sodium hydroxide solution from Fisher Scientific (USA) was used as the mobile phase solution.

2.2. Surfactant Adsorption. Surfactant stock solutions were prepared at predetermined concentrations of TMA, BTMA, and DDTMA in distilled deionized water. Batch adsorption experiments were conducted in a 50 mL amber glass bottle. To achieve a final ionic concentration of 10^{-2} M, 20 mL of deionized water, followed by 0.5 mL of a 1.0 M NaCl solution, was added to each bottle. Then, 0.1 g of ACC was added to each bottle and kept hydrating for one hour. To attain the desired concentrations, a predetermined quantity of surfactant stock solution was added, and pH was adjusted using 0.1 M, HCl, and NaOH solutions while maintaining the final sample volume at 50 mL. The adsorption reaction reached equilibrium within 8 h. The samples were then agitated on the reciprocal shaker for 10 h, and the residual surfactant content was determined in terms of total organic carbon content (TOC) by filtering 10 mL of solution aliquots with a Millex 5-m PVDF syringe-type filter (Millipore P/N SLSV025LS). The surfactants adsorbed on the ACC surface were calculated by dividing the difference between the final and initial concentrations by the ACC concentration.

2.3. Perchlorate Adsorption. The functionalized ACC was prepared by dispersing 0.03 g of ACC in 50 mL of a predetermined ClO_4^- concentration in perchlorate adsorption experiments. After 24 h of adsorption, the ClO_4^- concentration was recorded periodically using an ion chromatograph (Dionex 500) by withdrawing small aliquots (2 mL) of perchlorate at varied time intervals. The functionalized ACC was then rinsed three times with distilled deionized water to remove superficially adsorbed surfactants and dried in the oven at 38°C for 24 h. The as-prepared samples were cooled down and then placed in a desiccator before use. Adsorptions of perchlorate on functionalized ACC were carried out in batch experiments using the same methodology as the adsorption of cationic surfactants. All the experiments with the adsorption of fluoride by either pristine or functionalized ACC were performed in duplicate to assure reproducibility, and the adsorption values shown in this work are the average of two samples at different conditions.

2.4. Characterization. The Brunauer-Emmett-Teller (BET) model is used to determine the specific surface areas of all samples from surface measurements performed with the ASAP 2020 (Micromeritics), and the pore size distribution was calculated from the desorption branch using the Barrett-Joyner-Halenda (BJH) technique.

3. Computational Methods

3.1. Adsorption Energies between Single Surfactant Molecule and Graphite Model. The adsorption energies between surfactant molecules and the ACC substrate are calculated using semiempirical quantum mechanics (SQM). The molecular adsorption is modeled as a barrier-less exothermic reaction, and the adsorption energy is obtained from calculating the binding energy using the following equation:

$$E_{\text{ads}} = E_{\text{complex}} - (E_{\text{substrate}} + E_{\text{surfactant}}), \quad (1)$$

where E_{complex} is the minimal potential energy of the complex in vacuum mum, and $E_{\text{substrate}}$ and $E_{\text{surfactant}}$ represent the energies of the substrate and the surfactant separated at an infinite distance.

The calculation of adsorption energy was based on the procedure reported previously [37]. First, the graphite model went through energy minimization in a vacuum with the z-coordinate of all graphite atoms fixed at zero. Then, a single surfactant molecule was placed at the center of the graphite model. After optimizing the geometry of the surfactant with all graphite atoms fixed in space, E_{complex} was obtained. $E_{\text{surfactant}}$ and $E_{\text{substrate}}$ were then determined as single-point energies by separating the surfactant and graphite models

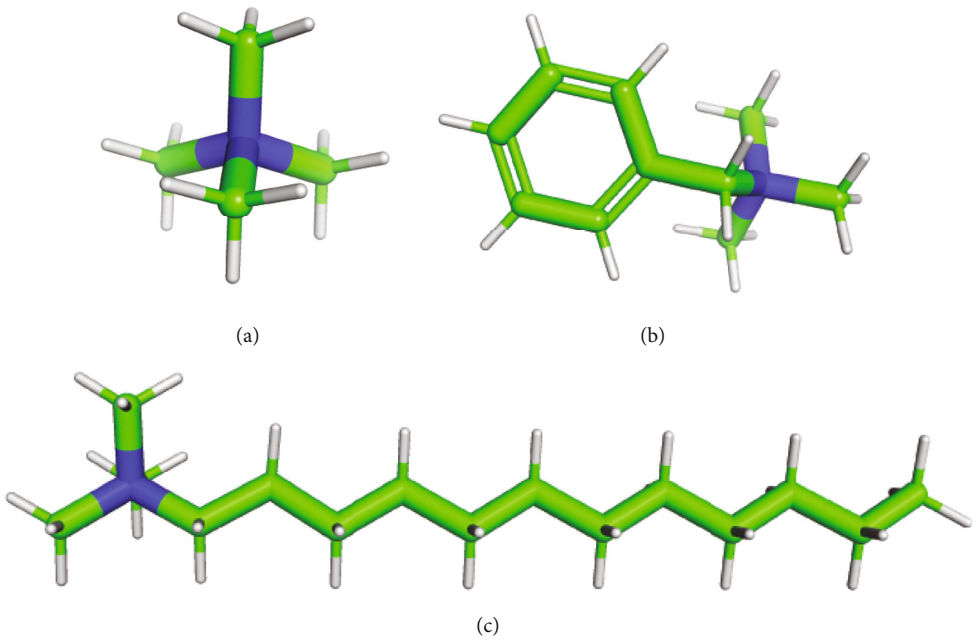

Figure 1: The molecular structure of cationic surfactants was used in this work. (a) TMA, (b) BTMA, and (c) DDTMA. Color codes: carbon atoms in green, hydrogen atoms in white, and nitrogen atoms in blue. Molecular structures are visualized using PyMOL [36].

at an infinite distance. The adsorption energies at the SQM level were calculated using the GFN2-xTB method [38] and a squared graphite model including 504 carbon atoms with hydrogen atoms to saturate the valence of edge carbons, as shown in Figure 2(a).

3.2. Simulations of Surfactant-Perchlorate Mixtures on a Graphite Surface. Molecular dynamics (MD) simulations were performed to understand the mechanism of different surfactant-ClO_4^- adsorption behaviors at the atomic level. The system setup is shown in Figures 2(b) and 2(c). The squared graphite surface is comprised of 1056 neutral carbon atoms with the dimensions $X = Y \cong 54$ Å. Initially, positively charged surfactant molecules with random orientation were added within 5 Å above the graphite surface. Then the water molecules and counter-ions were added to the system to make the concentrations of 0.275/0.55/0.825 M. The actual numbers of each species are listed in Table 1. Initial structures for simulations were prepared using Packmol [39]. A liquid-vapor interface is formed ~50 Å above the graphite surface depending on the surfactant and concentration of the solution. Periodic boundary conditions were applied, but the z-dimension was extended to 100 Å (see Figure 2(c)); therefore, only one liquid-solid interface is formed in each system.

All simulations were conducted in the NVT ensemble using NAMD 2.14 [40] with the CHARMM 36 and CGenFF force field parameters [41, 42]. Carbon atoms in the rigid graphite surface are modeled as neutral Lennard–Jones (LJ) spheres with the atom type CG2R61 (aromatic carbon) and are fixed throughout the simulations. We use TIP3P [43] water with SHAKE [44] to enforce the rigid water geometry. The particle mesh Ewald (PME) [45] method with a grid of 1.0 Å resolution and the Langevin method with a damping coefficient of 5 ps^{-1} were used to treat long-range electrostatic interactions and to fix the temperature at 300 K. The Lennard–Jones interactions were switched off gradually over the range of 10 and 11 Å. The equations of motion were integrated with a time step of 2.0 fs.

For each surfactant-ClO_4^- system and each concentration, we have at least 5 independent simulation runs with different initial structures and different seed numbers. Each simulation run is 10 ns with snapshots saved every 10 ps for further analyses. The first 5 ns of each run are treated as equilibration. The total sampling time for each system was between 25 and 50 ns.

4. Results and Discussion

4.1. Surfactant Adsorption on Activated Carbon Cloth. The adsorption isotherm of different surfactants on the activated carbon cloth (ACC) is provided in Figure 3. It shows that the adsorption capacity is significantly influenced by the chemical moieties of surfactants. All the isotherms in Figure 3 exhibit a sharp increase in adsorption followed by a single plateau that can be fitted to the Langmuir model [46] using the following equation:

$$\Gamma = \Gamma_{\max} \frac{K_L C_e}{1 + K_L C_e}, \tag{2}$$

where Γ is the amount of adsorbed surfactants (mmol/g), $\Gamma_{\max}$ represents the monolayer coverage capacity (mmol/g), K_L is the equilibrium constant (L/mmol), and C_e is the equilibrium concentration in solution (mM). Table 2 enlists the fitted parameters of the Langmuir equation. The values of

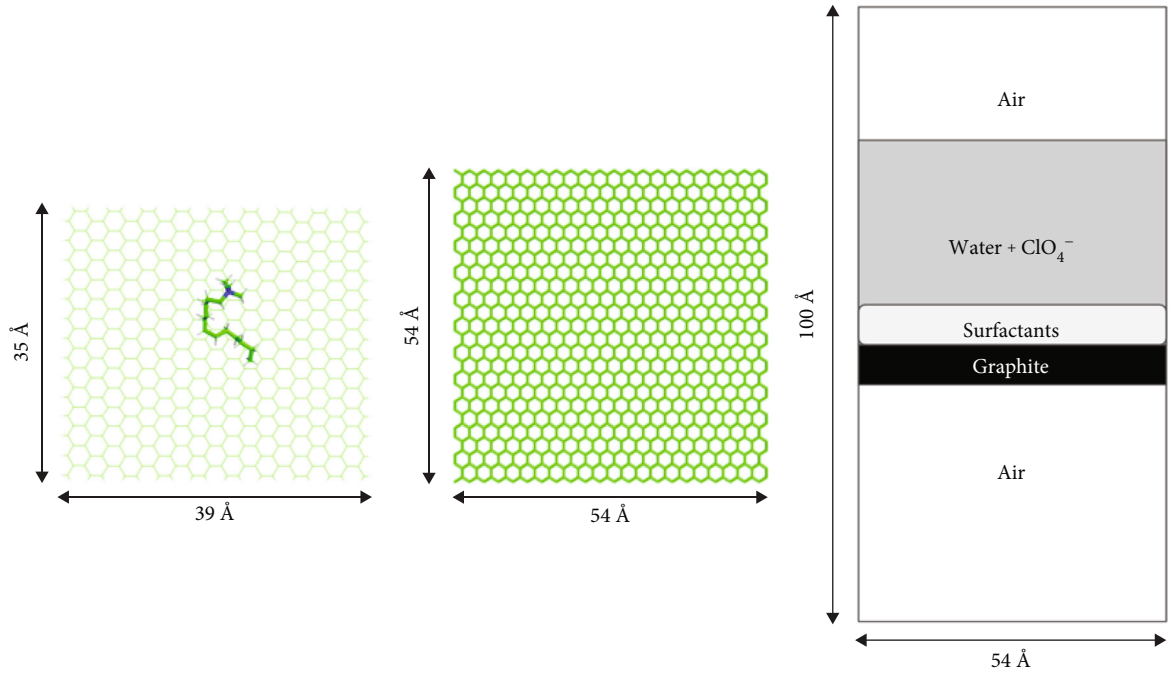

Figure 2: Systems used in adsorption energy calculations and MD simulations. (a) For adsorption energy calculations: graphite model (504 carbon atoms) with a preoptimized single molecule, (b) graphite model (1056 carbon atoms), and (c) illustration of the starting structure for MD simulations. Carbon atoms on graphite are fixed throughout the adsorption energy calculations and MD simulations. Molecular models were visualized with PyMOL [36].

Table 1: System setup of surfactant-perchlorate solutions at different concentrations for MD simulations.

Concentration (M)	N_{water}	$N_{surfactant}$	$N_{perchlorate}$
0.275	3920	20	20
0.550	3920	40	40
0.825	3920	60	60

Γ_{max} and K_L are in the order of DDTMA > BTMA > TMA. Results show that extended alkyl chains and aromatic rings facilitate the adsorption of surfactants on the ACC, particularly for DDTMA. The higher Γ_{max} suggests that the 12 alkyl chains in DDTMA can increase the affinity of surfactant towards the ACC surface, which is potentially contributed by the strong hydrophobicity of DDTMA [11, 47]. Moreover, a high value of K_L is also obtained in DDTMA (Table 2). This result indicates that the DDTMA surfactants are adsorbed more strongly on the surface of ACC compared to BTMA and TMA, which supports the findings that hydrophobic forces are more dominant for surfactant adsorption.

Additionally, the adsorption-free energy, ΔG_{ads}, was calculated based on K_L using Eq. (3) [48, 49].

$$\Delta G_{ads} = -\mathrm{RT}\ln K_L, \quad (3)$$

where R and T are the temperature and ideal gas constant, respectively, and the corresponding values of adsorption-free energy are reported in Table 2. Results demonstrated that all three surfactants provided a negative ΔG_{ads} value, indicating a spontaneous adsorption process onto the ACC surface under experimental conditions. Moreover, DDTMA exhibited the most negative ΔG_{ads}, revealing a stronger bonding tendency.

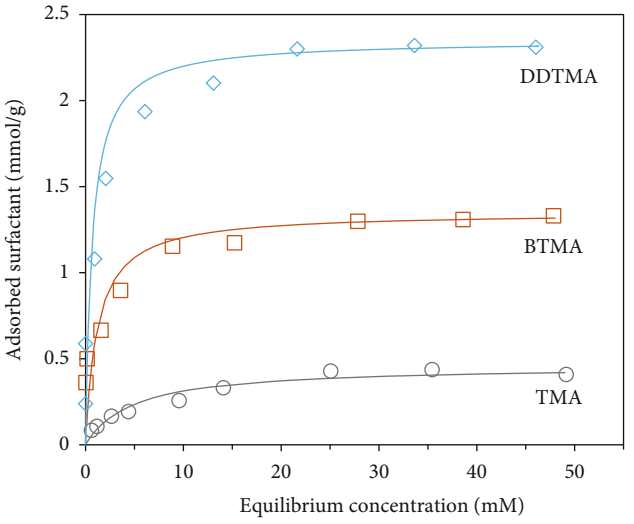

Figure 3: Adsorption of different surfactants on ACC. Experimental conditions: pH = 7, ionic strength = 10^{-2} M, the concentration of ACC = 1.4 g/L. Lines represent fits by the Langmuir model.

Table 2: Isotherm-fitted parameters for the adsorption of different surfactants.

System	Chemical formula	Γ_{max} (mmol/g)	K_L (L/mmol)	ΔG_{ads} (KJ/mol)
TMA	$(CH_3)_4N^+$	0.46	0.21	-13.2
BTMA	C_6H_5-CH_2N^+ $(CH_3)_3$	1.35	0.83	-16.7
DDTMA	CH_3-$(CH_2)_{11}N^+(CH_3)_3$	2.35	1.46	-18.1

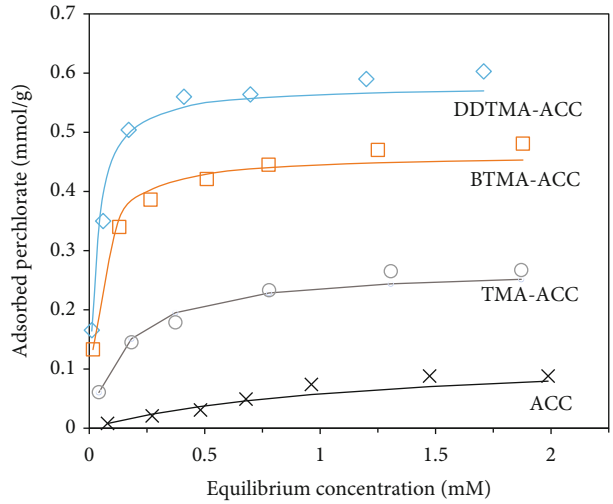

Figure 4: Adsorption of perchlorate on pristine and functionalized carbon cloth. Experimental conditions: [ACC] = 0.6 g/L, $I = 10^{-2}$ M NaCl, surface loading of surfactants = 0.4 mmol/g.

4.2. Perchlorate Adsorption on Functionalized Activated Carbon Cloth. In this work, the surfactant loading on functionalized ACCs for ClO_4^- adsorption is fixed at *ca.* 0.4 mmol/g. This specific mass loading is employed to prevent the influence of micelle aggregation during the surfactant loading process. The critical micelle concentration (CMC) for TMA [50], BTMA [51], and DTMA [52] is 5.4-5.7 mM, 110 mM, and 15 mM, respectively. It was reported that when the concentration of the surfactant is lower than its CMC, the surfactant molecules adsorbing onto the ACC surface exist primarily as monomers [53]. Therefore, the surfactant loading of 0.4 mmol/g on ACC presents an ideal platform to study the interactions among ACC, ClO_4^-, and various chemical moieties of cationic surfactants.

The ClO_4^- adsorption isotherms of pristine and functionalized ACCs are shown in Figure 4, and the corresponding fitted parameters for the Langmuir model are reported in Table 3. All three modified ACCs exhibit an increase in adsorption capacities compared to the pristine ACC. The maximum adsorption capacity of ClO_4^- is obtained in DDTMA-ACC, which is about 4.5 times higher than the performance of pristine ACC. Additionally, DDTMA-ACC presents the largest equilibrium adsorption constant K_L and the most negative ΔG_{ads}, indicating a stronger affinity for ClO_4^- towards ACC functionalized by DDTMA than that by other surfactants.

To explore the influence of surface modification on the performance of ClO_4^- adsorption, the surface properties of pristine and functionalized ACCs were examined. The BET-specific surface area is detailed in Table 3. The functionalization process is found to slightly decrease the surface area of ACC. The nitrogen adsorption–desorption isotherms of all ACCs are demonstrated in Figure S1. The obtained hysteresis loop exhibits a type-I pattern, suggesting the ACCs are mainly microporous solids [54]. The pore volume of samples decreased from 0.052 cm^3/g for pristine ACC to 0.04 cm^3/g for BTMA-ACC and DDTMA-ACC. The reduction of pore volume along with decreased surface area suggests that the surfactants were successfully adsorbed on the ACC surface but in different packing behaviors, thereby influencing their pore structure.

The characterization results clearly demonstrate that the functionalization of ACCs with various surfactants changes their surface properties including specific surface area, pore volume, and pore diameter. However, these features, such as reduced surface area, are difficult to explain the promoted adsorption capability of modified ACC and to reflect the impact of different surfactants on the adsorption performance [55]. To better understand the adsorption mechanisms of ClO_4^- in these ACC materials, MD simulations are employed to investigate the interactions among ClO_4^-, ACC, and various surfactants used in this work.

4.3. Adsorption Behavior of Surfactants Using In Silico Methods

4.3.1. Adsorption Energy between a Single Surfactant and the Graphite Surface. Initially, the adsorption energies among surfactants, perchlorate, and a model graphite surface were

Table 3: Physical properties of various ACC adsorbents and their isotherm-fitted parameters for the adsorption of perchlorate.

System	Surfactant loading (mmol/g)	Surface area (m^2/g)[a]	Pore volume (cm^3/g)[b]	Pore diameter (nm)[c]	Γ_{max} (mmol/g)	K_L (L/mmol)	ΔG_{ads} (KJ/mol)
Pristine ACC	—	1222	0.052	2.91	0.13	0.848	-16.7
TMA-ACC	0.43	1009	0.043	2.76	0.27	6.897	-21.9
BTMA-ACC	0.40	1110	0.040	2.67	0.46	25.28	-25.1
DDTMA-ACC	0.39	1053	0.040	2.76	0.59	35.90	-26.0

[a]N_2 adsorption isotherm at 77 K using the BET method. [b]Desorption cumulative volume of pores using the BJH method. [c]Desorption average pore diameter using the BJH method.

analyzed, and the results for TMA, BTMA, and DDTMA are shown in Table 4. The adsorption energies computed using DFT, force field, and GFN2-xTB techniques for other molecules in the supplementary information (Table S1) are benchmarks. For short-chain alkanes (methane and ethane), all three methods are within 1 kcal/mol differences from the experimental values. However, for aromatic compounds (benzene, naphthalene, and o-dichlorobenzene), differences of all methods are still within 2 kcal/mol, with the force field method showing a larger deviation from the experimental values. With regard to the gas/solvent molecules (methanol, ammonia, and water), all methods significantly underestimate the adsorption energies. The possible reasons have been discussed elsewhere [32] and are out of the scope of this manuscript. Based on the values reported for these molecules, we conclude that the performance of the GFN2-xTB SQM method has a good balance between efficiency and accuracy for adsorption energy calculations.

The calculated adsorption energies for TMA, BTMA, and DDTMA qualitatively reproduce the trend of the experimentally fitted ΔG_{ads} in Table 2. For BTMA, the optimized structure shows an orientational preference for the aromatic ring to be nearly parallel to the graphite surface with a ~90 kcal/mol difference from the dihedral angle scanning of the CH_2-aromatic ring bond (shown in Figure S2). As for DDTMA, there are more conformations than TMA and BTMA due to its longer chain length. The conformation with the lowest energy is extended with a distance of 15.3 Å between the nitrogen atom and terminal CH_3 (as shown in Figure 1(c)). We use the vector from nitrogen to the terminal CH_3 ($\overrightarrow{(NC)}$) to define the angle with the graphite surface and examine the interaction energies at different angles, as shown in Figure S3. The interaction energy shows a minimum when DDTMA is parallel to the graphite surface.

In practice, we rarely have only one surfactant molecule interacting with the graphite surface as in adsorption energy calculations. While multiple surfactant molecules have interactions with each other, they also interact with the perchlorate, which may lead to different adsorption behaviors.

4.3.2. Number Density Profile of Perchlorate and Surfactant Ions with the Graphite Surface. We use atomistic molecular dynamics simulations to mimic multibody interactions and analyze the adsorption behaviors of different surfactant-perchlorate systems. The number density profiles of cations/surfactants and perchlorate along the z-dimension relative to the graphite surface are shown in Figure 5. The number density is defined as

Table 4: Calculated adsorption energy between surfactant and graphite surface using the GFN2-xTB methods. All values are in kcal/mol.

Molecule	E_a
TMA	-20.19
BTMA	-26.62
DDTMA	-35.52

$$\rho(z) = \frac{N(z)}{L_x L_y \Delta z}, \tag{4}$$

where L_x and L_y represent the length of x- and y-dimensions in the simulations. Δz represents the unit length in z-dimension of each volume slab, with $N(z)$ denoting the number of species within this slab. In each panel, the total area under each curve/species equals 1.

We first focus on the number density profiles of Na^+/surfactants as $\boldsymbol{\rho}_{cation}(z)$. We use the positions of the nitrogen atoms in the surfactant molecules to represent the corresponding positions in these calculations since the nitrogen atoms carry most of the positive charges. Na^+ shows no preference near the graphite surface in all concentrations (Figures 5(a)–5(c)). TMA shows two peaks at $z = 4$ and 7.5 Å (Figures 5(d)–5(f)), with the peaks both becoming more evident as the concentration increases. BTMA shows a strong first peak at $z = 5$ Å, with a weak second peak only shown in the highest concentration (Figures 5(g)–5(i)). In the case of DDTMA, there is only one strong peak at 0.275 M (Figure 5(j)); as the concentration elevates, the second peak becomes more evident with an extremely long tail (Figures 5(k) and 5(l)).

With regard to the number density profiles of perchlorate $\boldsymbol{\rho}_{anion}(z)$, when the counter-ion is Na^+, ClO_4^- still shows some surface activity with a peak at $z = 3.8$ Å. When the surfactant is TMA, the ClO_4^- adsorption peaks are enhanced relative to the cases of Na-ClO_4 at all concentrations. This adsorption peak enhancement is more evident in the BTMA-ClO_4 systems. In the case of DDTMA as the surfactant, the ClO_4^- adsorption peak is slightly enhanced

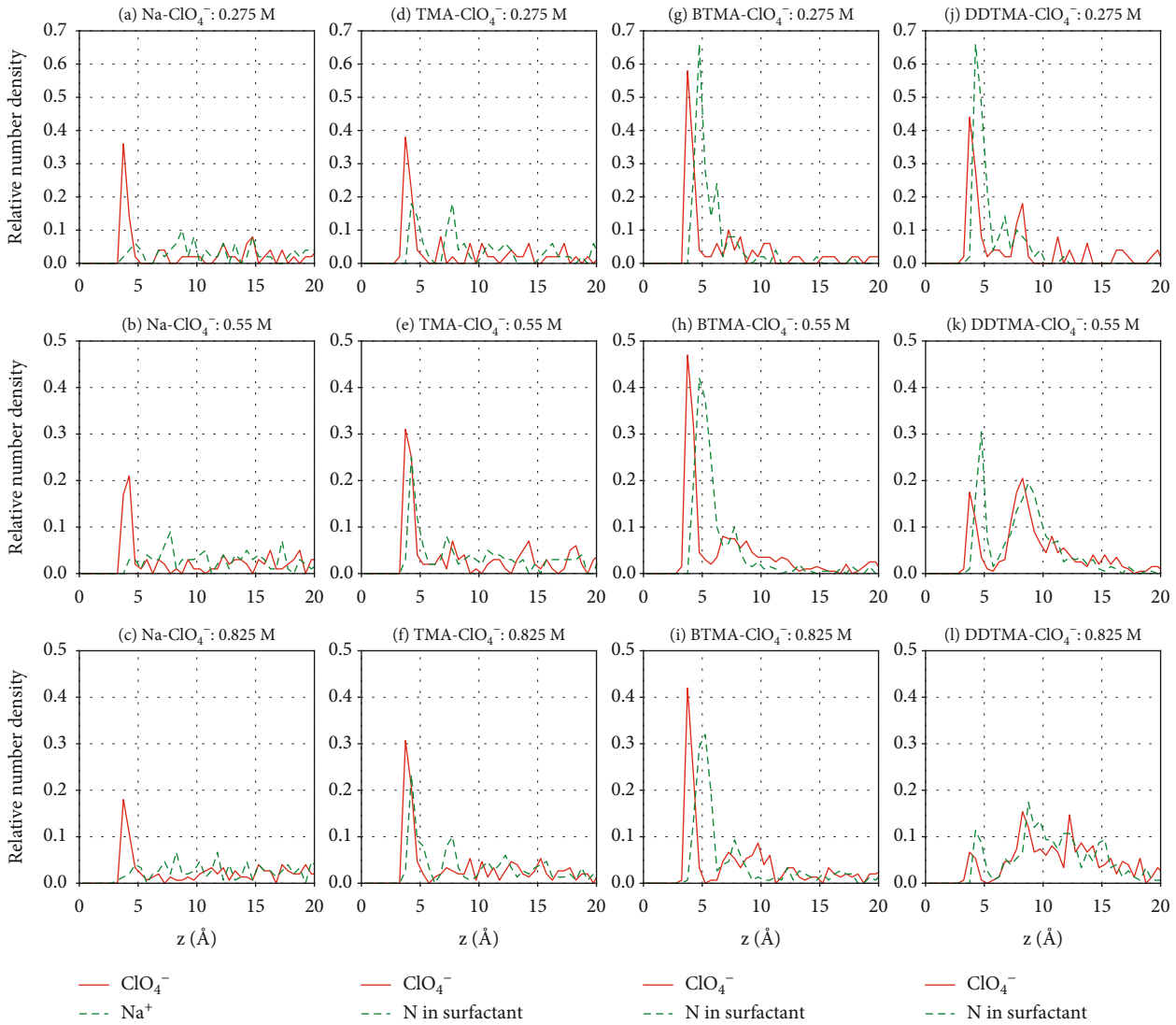

FIGURE 5: Relative number density profiles of perchlorate/surfactants along the z-direction from the graphite surface. The total area under each curve/species equals 1.

compared to the Na-ClO_4 system at low concentration; as the concentration increases, the ClO_4^- adsorption peak becomes even weaker than the Na-ClO_4 system. While other surfactants such as TMA/BTMA tend to show strong peaks/single-layered packing behavior near the graphite surface, DDTMA shows relatively flattened (or multilayered, contrary to the single-layered) adsorption behaviors from the graphite surface. We further investigate this effect by plotting cumulative numbers of ClO_4^- and Na^+/surfactants as functions of relative z-positions in Figure 6. The cumulative number $Q(z)$ is defined as follows:

$$Q(z) = N_{\text{total}} \times \int_0^z \rho(z)dz, \tag{5}$$

where N_{total} is the total number of anion-cation pairs at each concentration; therefore, $Q(z) = N_{\text{total}}$ when z equals infinity. For all species in our systems, $Q(z)$ reaches N_{total} at $z = 50$ Å. We use $z = 15$ Å as the distance cutoff to inspect each $Q(z)$, as listed in Table 5. When concentration = 0.275 M, Q_{anion} and Q_{cation} in both BTMA-ClO_4 and DDTMA-ClO_4 systems are similar (Q_{anion}~15 and Q_{cation} ~20). At concentration = 0.55 M, we start to see the amount of DDTMA ($Q_{\text{cation}} = 38.7$) to be significantly larger than BTMA ($Q_{\text{cation}} = 32.6$), while both Q_{anion} are ~32. Both Q_{anion} and Q_{cation} in DDTMA-ClO_4 are larger than Q_{anion} and Q_{cation} in BTMA-ClO_4 at the highest concentration. Despite being the largest surfactant in this study, DDTMA molecules show the stronger capability to pack themselves within identical volumes ($z = 15$ Å in our case). For surfactants like TMA/BTMA, they can only form a single layer near the graphite surface, while the rest of the surfactants are further away from the surface, which consequently reduces the adsorption of perchlorate anions. On the other hand, most DDTMA molecules reside near the graphite surface, thus inducing more perchlorate anion adsorption.

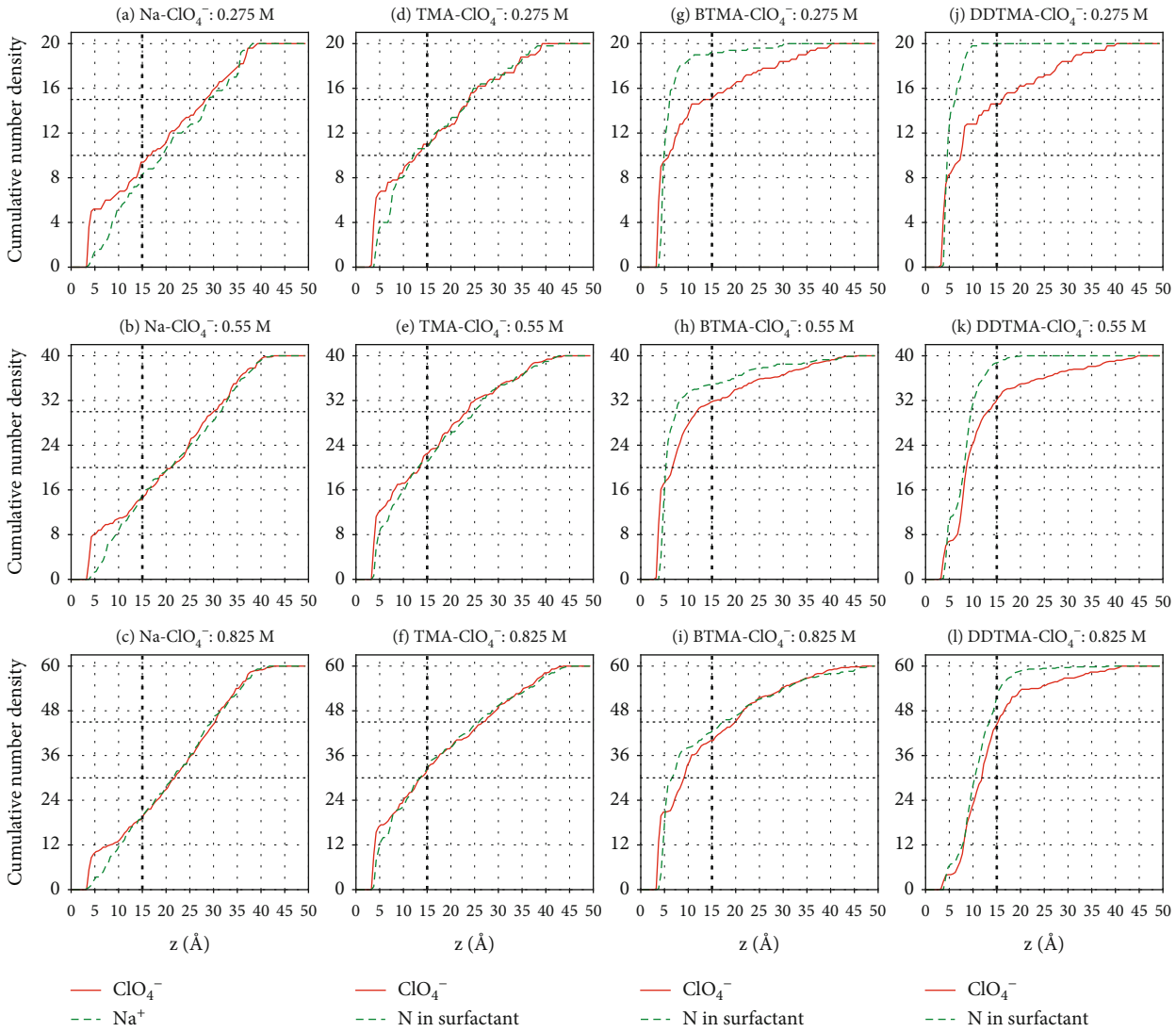

Figure 6: Cumulative number (Q) of perchlorate/surfactants along the z-dimension from the graphite surface. Each curve represents one species and eventually approaches the total number of ion pairs in the system. Dotted lines in each panel represent $Q(z)$ at $z = 15$ Å.

Table 5: $Q(z)$ when $z = 15$ Å for each species in each system.

System	Concentration (M)	N_{total}	Q_{anion} (15 Å)	Q_{cation} (15 Å)
Na-ClO_4	0.275	20	9.4	8.4
	0.550	40	14.4	14.8
	0.825	60	19.0	19.6
TMA-ClO_4	0.275	20	11.0	10.6
	0.550	40	22.6	21.2
	0.825	60	32.6	32.6
BTMA-ClO_4	0.275	20	15.0	19.2
	0.550	40	32.6	32.6
	0.825	60	40.0	42.4
DDTMA-ClO_4	0.275	20	14.6	20.0
	0.550	40	31.7	38.7
	0.825	60	43.9	51.6

5. Conclusions

Activated carbon cloth is successfully functionalized using surfactant adsorption for perchlorate removal. A constant surfactant loading of 0.4 mmol/g is used to prevent micelle aggregation and to analyze the interaction among ACC, ClO_4^-, and various cationic surfactants. The adsorption of the surfactants on the surface of the ACC is confirmed by a decrease in pore volume and an increase in surface area. Regardless of the nature of the surfactants, high functionality and perchlorate removal efficiency compared with pristine ACC are obtained. Of the most significant, DDTMA-ACC demonstrates about 350% improvement in the ClO_4^- adsorption compared to pristine ACC. DDTMA-ACC also outperforms BTMA-ACC and TMA-ACC with a 30% and 120% increase in Γ_{max}, respectively. Further, MD simulation studies reveal that the enhanced ClO_4^- adsorption capability of DDTMA-ACC is attributable to the closely packed or multilayered packing features of DDTMA on the ACC surface. It is found that minimal interaction energy occurs when DDTMA is parallel with the model graphite surface. Relative number density profiles and cumulative number studies further demonstrate that the majority of DDTMA molecules reside near the graphite surface, whereas TMA/BTMA can only form a single layer, which deteriorates the adsorption performance. Our joint experiment-simulation study offers a new route to elucidate the underlying mechanism of surfactant-based surface modification and enable a transformative impact on material design to surpass the performance of conventional perchlorate adsorbents for wastewater treatment.

Data Availability

The data used to support the findings of this study are available from the corresponding author upon request.

Conflicts of Interest

The authors declare that they have no known competing financial interests or personal relationships that could have appeared to influence the work reported in this paper.

Acknowledgments

The authors acknowledge the financial support from the National Science and Technology Council of Taiwan with grant numbers 109-2222-E-131-002-MY3, 110-2222-E-182-002-MY3, 112-2628-E-182-001-MY3, and 112-2221-E-131-007. W.-F. K. and C.-L. C. also express gratitude for the financial support provided by Chang Gung University (URRPD2N0041).

Supplementary Materials

Figure S1: nitrogen adsorption–desorption isotherms of various adsorbents. Figure S2: relative energy profile for different orientations between BTMA and graphite surface. Figure S3: relative energy profile for different orientations of DDTMA. Table S1: calculated adsorption energies to graphite using CGenFF force field, DFT, and semiempirical GFN2-xTB methods. *(Supplementary Materials)*

References

[1] K.-L. Chen, M. S. Ahmad, and C.-L. Chen, "Enhanced nitrate reduction over functionalized Pd/Cu electrode with tunable conversion to nitrogen and sodium hydroxide recovery," *Science of the Total Environment*, vol. 869, p. 161849, 2023.

[2] P. F. Lito, J. P. Aniceto, and C. M. Silva, "Removal of anionic pollutants from waters and wastewaters and materials perspective for their selective sorption," *Water, Air, & Soil Pollution*, vol. 223, no. 9, pp. 6133–6155, 2012.

[3] R. Baby, M. Z. Hussein, Z. Zainal, and A. H. Abdullah, "Preparation of functionalized palm kernel shell bio-adsorbent for the treatment of heavy metal-contaminated water," *Journal of Hazardous Materials Advances*, vol. 10, article 100253, 2023.

[4] Y. Xie, L. Ren, X. Zhu, X. Gou, and S. Chen, "Physical and chemical treatments for removal of perchlorate from water-a review," *Process Safety and Environmental Protection*, vol. 116, pp. 180–198, 2018.

[5] R. A. Clewell, E. A. Merrill, K. O. Yu et al., "Predicting neonatal perchlorate dose and inhibition of iodide uptake in the rat during lactation using physiologically-based pharmacokinetic modeling," *Toxicological Sciences*, vol. 74, no. 2, pp. 416–436, 2003.

[6] B. De Groef, B. R. Decallonne, S. Van der Geyten, V. M. Darras, and R. Bouillon, "Perchlorate versus other environmental sodium/iodide symporter inhibitors: potential thyroid-related health effects," *European Journal of Endocrinology*, vol. 155, no. 1, pp. 17–25, 2006.

[7] J. Wolff, "Perchlorate and the thyroid gland," *Pharmacological Reviews*, vol. 50, no. 1, pp. 89–105, 1998.

[8] D. R. Lobato-Peralta, E. Duque-Brito, A. Ayala-Cortés et al., "Advances in activated carbon modification, surface heteroatom configuration, reactor strategies, and regeneration methods for enhanced wastewater treatment," *Journal of Environmental Chemical Engineering*, vol. 9, no. 4, p. 105626, 2021.

[9] W. Chen, F. S. Cannon, and J. R. Rangel-Mendez, "Ammonia-tailoring of GAC to enhance perchlorate removal. II: perchlorate adsorption," *Carbon*, vol. 43, no. 3, pp. 581–590, 2005.

[10] Y. Cui and J. D. Atkinson, "Tailored activated carbon from glycerol: role of acid dehydrator on physiochemical characteristics and adsorption performance," *Journal of Materials Chemistry A*, vol. 5, no. 32, pp. 16812–16821, 2017.

[11] R. Mahmudov, C. Chen, and C.-P. Huang, "Functionalized activated carbon for the adsorptive removal of perchlorate from water solutions," *Frontiers of Chemical Science and Engineering*, vol. 9, no. 2, pp. 194–208, 2015.

[12] R. Mahmudov and C. P. Huang, "Perchlorate removal by activated carbon adsorption," *Separation and Purification Technology*, vol. 70, no. 3, pp. 329–337, 2010.

[13] B. Rai, P. Sathish, J. Tanwar, K. Moon, and D. Fuerstenau, "A molecular dynamics study of the interaction of oleate and dodecylammonium chloride surfactants with complex aluminosilicate minerals," *Journal of Colloid and Interface Science*, vol. 362, no. 2, pp. 510–516, 2011.

[14] N. R. Tummala, L. Shi, and A. Striolo, "Molecular dynamics simulations of surfactants at the silica-water interface: anionic vs nonionic headgroups," *Journal of Colloid and Interface Science*, vol. 362, no. 1, pp. 135–143, 2011.

[15] Y. Xia, R. Zhang, Y. Xing, and X. Gui, "Improving the adsorption of oily collector on the surface of low-rank coal during flotation using a cationic surfactant: an experimental and molecular dynamics simulation study," *Fuel*, vol. 235, pp. 687–695, 2019.

[16] L. Xu, H. Wu, F. Dong, L. Wang, Z. Wang, and J. Xiao, "Flotation and adsorption of mixed cationic/anionic collectors on muscovite mica," *Minerals Engineering*, vol. 41, pp. 41–45, 2013.

[17] Y. Xu, Y.-L. Liu, D.-D. He, and G.-S. Liu, "Adsorption of cationic collectors and water on muscovite (0 0 1) surface: a molecular dynamics simulation study," *Minerals Engineering*, vol. 53, pp. 101–107, 2013.

[18] L. Zhang, B. Li, Y. Xia, and S. Liu, "Wettability modification of Wender lignite by adsorption of dodecyl poly ethoxylated surfactants with different degree of ethoxylation: a molecular dynamics simulation study," *Journal of Molecular Graphics and Modelling*, vol. 76, pp. 106–117, 2017.

[19] J. Tang, A. Ahmadi, A. a. Alizadeh et al., "Investigation of the mechanical properties of different amorphous composites using the molecular dynamics simulation," *Journal of Materials Research and Technology*, vol. 24, pp. 1390–1400, 2023.

[20] X. Lyu, X. You, M. He et al., "Adsorption and molecular dynamics simulations of nonionic surfactant on the low rank coal surface," *Fuel*, vol. 211, pp. 529–534, 2018.

[21] S. Majidi, H. Erfan-Niya, J. Azamat, S. Ziaei, E. R. Cruz-Chú, and J. H. Walther, "Membrane based water treatment: insight from molecular dynamics simulations," *Separation & Purification Reviews*, vol. 52, no. 4, pp. 336–352, 2023.

[22] H. Ouachtak, A. El Guerdaoui, R. El Haouti et al., "Combined molecular dynamics simulations and experimental studies of the removal of cationic dyes on the eco-friendly adsorbent of activated carbon decorated montmorillonite Mt@ AC," *RSC Advances*, vol. 13, no. 8, pp. 5027–5044, 2023.

[23] S. Majidi, H. Erfan-Niya, J. Azamat, E. R. Cruz-Chú, and J. H. Walther, "The separation performance of porous carbon nitride membranes for removal of nitrate and nitrite ions from contaminated aqueous solutions: a molecular dynamics study," *Colloids and Surfaces A: Physicochemical and Engineering Aspects*, vol. 655, p. 130208, 2022.

[24] J. O. Eniola, B. Sizirici, Y. Fseha, J. F. Shaheen, and A. M. Aboulella, "Application of conventional and emerging low-cost adsorbents as sustainable materials for removal of contaminants from water," *Environmental Science and Pollution Research*, vol. 30, no. 38, pp. 88245–88271, 2023.

[25] R. B. Kalengyo, M. G. Ibrahim, M. Fujii, and M. Nasr, *Utilizing orange peel waste biomass in textile wastewater treatment and its recyclability for dual biogas and biochar production: a techno-economic sustainable approach*, Biomass Conversion and Biorefinery, 2023.

[26] N. Siva Kumar, M. Asif, A. M. Poulose, E. H. Al-Ghurabi, S. S. Alhamedi, and J. R. Koduru, "Preparation, characterization, and chemically modified date palm fiber waste biomass for enhanced phenol removal from an aqueous environment," *Materials*, vol. 16, no. 11, p. 4057, 2023.

[27] F. Marrakchi, M. J. Ahmed, W. A. Khanday, M. Asif, and B. H. Hameed, "Mesoporous-activated carbon prepared from chitosan flakes via single-step sodium hydroxide activation for the adsorption of methylene blue," *International Journal of Biological Macromolecules*, vol. 98, pp. 233–239, 2017.

[28] W. A. Khanday, M. J. Ahmed, P. U. Okoye, E. H. Hummadi, and B. H. Hameed, "Single-step pyrolysis of phosphoric acid-activated chitin for efficient adsorption of cephalexin antibiotic," *Bioresource Technology*, vol. 280, pp. 255–259, 2019.

[29] M. A. Islam, S. Sabar, A. Benhouria, W. A. Khanday, M. Asif, and B. H. Hameed, "Nanoporous activated carbon prepared from karanj (*Pongamia pinnata*) fruit hulls for methylene blue adsorption," *Journal of the Taiwan Institute of Chemical Engineers*, vol. 74, pp. 96–104, 2017.

[30] M. A. Islam, M. J. Ahmed, W. A. Khanday, M. Asif, and B. H. Hameed, "Mesoporous activated carbon prepared from NaOH activation of rattan (*Lacosperma secundiflorum*) hydrochar for methylene blue removal," *Ecotoxicology and Environmental Safety*, vol. 138, pp. 279–285, 2017.

[31] W. A. Khanday, M. Asif, and B. H. Hameed, "Cross-linked beads of activated oil palm ash zeolite/chitosan composite as a bio-adsorbent for the removal of methylene blue and acid blue 29 dyes," *International Journal of Biological Macromolecules*, vol. 95, pp. 895–902, 2017.

[32] W. A. Khanday and B. H. Hameed, "Zeolite-hydroxyapatite-activated oil palm ash composite for antibiotic tetracycline adsorption," *Fuel*, vol. 215, pp. 499–505, 2018.

[33] W. A. Khanday, F. Marrakchi, M. Asif, and B. H. Hameed, "Mesoporous zeolite-activated carbon composite from oil palm ash as an effective adsorbent for methylene blue," *Journal of the Taiwan Institute of Chemical Engineers*, vol. 70, pp. 32–41, 2017.

[34] F. Marrakchi, W. A. Khanday, M. Asif, and B. H. Hameed, "Cross-linked chitosan/sepiolite composite for the adsorption of methylene blue and reactive orange 16," *International Journal of Biological Macromolecules*, vol. 93, no. Part A, pp. 1231–1239, 2016.

[35] M. J. Rosen and J. T. Kunjappu, *Surfactants and interfacial phenomena*, John Wiley & Sons, 2012.

[36] L. Schrödinger and W. DeLano, *PyMOL*, 2020, http://www.pymol.org/pymol.

[37] S. Conti and M. Cecchini, "Accurate and efficient calculation of the desorption energy of small molecules from graphene," *The Journal of Physical Chemistry C*, vol. 119, no. 4, pp. 1867–1879, 2015.

[38] C. Bannwarth, S. Ehlert, and S. Grimme, "GFN2-xTB—an accurate and broadly parametrized self-consistent tight-binding quantum chemical method with multipole electrostatics and density-dependent dispersion contributions," *Journal of Chemical Theory and Computation*, vol. 15, no. 3, pp. 1652–1671, 2019.

[39] L. Martínez, R. Andrade, E. G. Birgin, and J. M. Martínez, "PACKMOL: a package for building initial configurations for molecular dynamics simulations," *Journal of Computational Chemistry*, vol. 30, no. 13, pp. 2157–2164, 2009.

[40] J. C. Phillips, D. J. Hardy, J. D. Maia et al., "Scalable molecular dynamics on CPU and GPU architectures with NAMD," *The Journal of Chemical Physics*, vol. 153, no. 4, article 044130, 2020.

[41] K. Vanommeslaeghe, E. Hatcher, C. Acharya et al., "CHARMM general force field: a force field for drug-like molecules compatible with the CHARMM all-atom additive biological force fields," *Journal of Computational Chemistry*, vol. 31, no. 4, pp. 671–690, 2010.

[42] W. Yu, X. He, K. Vanommeslaeghe, and A. D. MacKerell Jr., "Extension of the CHARMM general force field to sulfonyl-containing compounds and its utility in biomolecular simulations," *Journal of Computational Chemistry*, vol. 33, no. 31, pp. 2451–2468, 2012.

[43] W. L. Jorgensen, J. Chandrasekhar, J. D. Madura, R. W. Impey, and M. L. Klein, "Comparison of simple potential functions for simulating liquid water," *The Journal of Chemical Physics*, vol. 79, no. 2, pp. 926–935, 1983.

[44] J.-P. Ryckaert, G. Ciccotti, and H. J. Berendsen, "Numerical integration of the Cartesian equations of motion of a system with constraints: molecular dynamics of *n*-alkanes," *Journal of Computational Physics*, vol. 23, no. 3, pp. 327–341, 1977.

[45] T. Darden, D. York, and L. Pedersen, "Particle mesh Ewald: AnN·log(N) method for Ewald sums in large systems," *The Journal of Chemical Physics*, vol. 98, no. 12, pp. 10089–10092, 1993.

[46] W. Ahmed, M. Booth, and E. Nourafkan, *Emerging nanotechnologies for renewable energy*, Elsevier, 2021.

[47] C.-L. Chen, S.-W. Park, J. F. Su et al., "The adsorption characteristics of fluoride on commercial activated carbon treated with quaternary ammonium salts (Quats)," *Science of the Total Environment*, vol. 693, article 133605, 2019.

[48] R. Fuchs-Godec and V. Doleček, "A effect of sodium dodecylsulfate on the corrosion of copper in sulphuric acid media," *Colloids and Surfaces A: Physicochemical and Engineering Aspects*, vol. 244, no. 1-3, pp. 73–76, 2004.

[49] M. S. Walczak, P. Morales-Gil, and R. Lindsay, "Determining Gibbs energies of adsorption from corrosion inhibition efficiencies: is it a reliable approach?," *Corrosion Science*, vol. 155, pp. 182–185, 2019.

[50] M. Benrraou, B. L. Bales, and R. Zana, "Effect of the nature of the counterion on the properties of anionic surfactants. 1. Cmc, ionization degree at the cmc and aggregation number of micelles of sodium, cesium, tetramethylammonium, tetraethylammonium, tetrapropylammonium, and tetrabutylammonium dodecyl sulfates," *The Journal of Physical Chemistry B*, vol. 107, no. 48, pp. 13432–13440, 2003.

[51] Y. Gao, J. Chai, J. Xu, G. Li, and G. Zhang, "Dynamic surface tension and adsorption mechanism of surfactant benzyltrimethylammonium bromide at the air/water interface," *Journal of Dispersion Science and Technology*, vol. 27, no. 8, pp. 1059–1063, 2006.

[52] B. Bijsterbosch, "Characterization of silica surfaces by adsorption from solution. Investigations into the mechanism of adsorption of cationic surfactants," *Journal of Colloid and Interface Science*, vol. 47, no. 1, pp. 186–198, 1974.

[53] S.-Y. Lin, W.-f. Chen, M.-T. Cheng, and Q. Li, "Investigation of factors that affect cationic surfactant loading on activated carbon and perchlorate adsorption," *Colloids and Surfaces A: Physicochemical and Engineering Aspects*, vol. 434, pp. 236–242, 2013.

[54] C. Brasquet and P. Le Cloirec, "Effects of activated carbon cloth surface on organic adsorption in aqueous solutions. Use of statistical methods to describe mechanisms," *Langmuir*, vol. 15, no. 18, pp. 5906–5912, 1999.

[55] C.-L. Chen, Y.-J. Shih, J. F. Su, K.-L. Chen, and C.-P. Huang, "Mesoporous zirconium pyrophosphate for the adsorption of fluoride from dilute aqueous solutions," *Chemical Engineering Journal*, vol. 427, p. 132034, 2022.